Applied Catalysis B: Environmental 178 (2015) 29–36

Contents lists available at ScienceDirect

Applied Catalysis B: Environmental

journal homepage: www.elsevier.com/locate/apcatb

Removal of Rhodamine B with Fe-supported bentonite as heterogeneous photo-Fenton catalyst under visible irradiation

Yaowen Gao[a], Yan Wang[a,b], Hui Zhang[a,*]

[a] Department of Environmental Engineering, Wuhan University, PO Box C319, Luoyu Road No. 129, Wuhan 430079, China
[b] Department of Environmental Science and Engineering, Anhui Science and Technology University, Donghua Road No. 9, Fengyang 233100, China

ARTICLE INFO

Article history:
Received 12 July 2014
Received in revised form 1 November 2014
Accepted 3 November 2014
Available online 13 November 2014

Keywords:
Circumneutral pH
Degradation
Fe-supported bentonite
Visible light photo-Fenton
Rhodamine B

ABSTRACT

Fe-supported bentonite (Fe-B) was successfully fabricated as a low-cost heterogeneous catalyst for adsorption and visible light photo-Fenton degradation of Rhodamine B (RhB) from aqueous solution. The support of iron rendered a significant increase in specific surface area and a slight increase in interlayer spacing of bentonite, thus improving the adsorption performance of Fe-B. The maximum adsorption capacity of RhB onto Fe-B was calculated to be 227.27 mg g^{-1} by the fitting of Langmuir adsorption isotherm. The catalytic activity of Fe-B was evaluated by the degradation of RhB (80 mg L^{-1}) in the presence of H_2O_2 under visible light irradiation. Light-emitting diodes (LED) lamps were used as visible light source as they are small in size, energy efficient, compact, have a relatively long life span, and can be facile to operate. The estimated quantum yield of photodegradation of RhB was calculated as $(1.66 \pm 0.21) \times 10^{-2}$. The results showed that the Fe-B catalyst demonstrated good performance in the removal of RhB by combination of adsorption and degradation with optimum operating conditions of Fe-B 0.25 g L^{-1}, natural pH 4.2 and H_2O_2 12 mM. The Fe-B catalyst retained high visible light photocatalytic activity toward RhB in a wide pH range from 3.0 to 9.0 and exhibited good chemical stability after five consecutive adsorption/degradation cycles.

1. Introduction

Over the past decades, the treatment of textile and dyeing wastewater with severe color, low biodegradability and high toxicity has been one of the major concerns in environmental protection [1–3]. Rhodamine B (RhB) is a nitrogen-containing dye which appears to undergo natural reductive anaerobic degradation to yield potentially carcinogenic aromatic amines [4]. In order to eliminate the negative environmental impact of RhB, advanced oxidation processes (AOPs) was proposed as an alternative approach since conventional biological wastewater treatment processes are not efficient to remove RhB [5,6].

As an advanced oxidation process, titanium dioxide (TiO_2) photocatalysis has been successfully applied to the degradation of RhB [6,7]. Being a wide band-gap material, TiO_2 could absorb only ultraviolet light which accounts for merely approximately 4% of solar energy at the Earth's surface. This greatly limits its practical applications [8,9]. Thus, the visible light driven photocatalysts have been developed, including Bi_2WO_6 [10], boron-doped graphitic carbon nitride [11], Fe_3O_4@Bi_2O_3 [12], anionic (C, S, N) or cationic (Fe, V) doping of TiO_2 [13–15], and so on. Nevertheless, these photocatalysts are difficult to be available at a reasonable cost and the luminous energy consumption is usually relatively high [2,16,17]. Compared with other AOPs, Fenton's reagent is relatively inexpensive and Fenton process is easily operated and maintained [18]. Unfortunately, the drawbacks associated to the homogeneous process, namely the narrow acidic pH range and the formation of large amount of iron-containing sludge, limit the application of conventional Fenton process [19–23]. Therefore, many efforts have been made to employ heterogeneous Fenton catalysts for the incorporation of active iron species into various supports, such as crushed brick, activated alumina, zeolite, silica, grapheme oxide, etc. [24–30]. However, these supported catalysts are more or less unsatisfactory in terms of relatively low efficiency of hydrogen peroxide utilization, or being expensive of the starting material for Fenton catalysts. On account of the high specific surface area, clays are attractive as adsorbents [20,31,32]. Moreover, clays are natural, abundant, cheap and environment-friendly, which makes them good candidates as catalyst supports [20,33,34].

It was found that dyes can absorb visible light and become excited under visible irradiation. The subsequent electron transfer from the excited dye molecules to the Fe(III) species would enhance

* Corresponding author. Tel.: +86 27 68775837; fax: +86 27 68778893.
E-mail address: eeng@whu.edu.cn (H. Zhang).

http://dx.doi.org/10.1016/j.apcatb.2014.11.005
0926-3373/

Fenton chain reactions [35,36]. As a result, the iron-containing clays and iron supported clays have been employed as heterogeneous catalysts in the visible light photo-Fenton process for the degradation of RhB as well as other dyes [20,35–37]. The visible light sources used in these studies are mainly halogen lamps which have a relatively short life-span and high energy consumption, require cooling, and can be inconvenient to operate [38]. Compared to conventional light sources, light-emitting diode (LED) lamps are small in size, robust, environmentally friendly, which have relatively low costs but a longer life span [38]. More importantly, the LED lamps are not calorigenic, and then the reactions can be performed at room temperature without the use of cooling water [39]. Therefore, in this study, natural bentonite clay was used as support to synthesize photo-Fenton catalyst (Fe-supported bentonite, denoted as Fe-B) and LED lamps with a central wavelength of 455 nm were employed as visible light sources. The prepared catalyst was characterized by several spectroscopic techniques such as field-emission scanning electron microscopy (FESEM), energy dispersive spectra (EDS), small angle X-ray diffraction (SAXRD), and Fourier transform infrared spectroscopy (FTIR). The adsorption of RhB was firstly investigated under the operating conditions including initial dye concentration, Fe-B dosage and initial pH. Then the adsorption isotherm model was determined. Afterwards, the photocatalytic activity of Fe-B was evaluated on the degradation of RhB in the presence of H_2O_2 under LED irradiation. The effects of operating parameters such as initial solution pH and H_2O_2 dosage on the degradation of RhB were investigated. The stability and reusability of the catalyst were also explored.

2. Experimental

2.1. Materials

Natural bentonite was procured from Ezhou City, Hubei Province, China. RhB was purchased from Sinopharm Chemical Reagent Co., Ltd., China. All chemicals were of analytical grade and were used without any further purification. In the experiments, the solutions were prepared using deionized water.

2.2. Preparation of Fe-supported bentonite

The Fe-supported bentonite was prepared by a modified method described in the literature [37,40]. In a typical process, an aqueous solution of sodium carbonate was added drop wise to the solution of ferric nitrate under magnetic stirring at 25 °C until the molar ratio of $[Na^+]/[Fe^{3+}]$ was unity. Then the resulting solution was aged for 24 h at 25 °C. After that, a certain amount of bentonite was dispersed in the above resulting solution under magnetic stirring at 60 °C such that a ratio of 10 mmol Fe/g of bentonite was established. The suspension was stirred for 6 h followed by aging at 60 °C for 24 h. Afterwards, the precipitate was separated from the mixture by centrifugation and washed with deionized water. Then, it was dried at a given temperature (typically at 100 °C) in air overnight and finally the Fe-B catalyst was obtained.

2.3. Catalyst characterization

Specific surface area (S_{BET}) of samples was determined by the N_2 Brunauer–Emmett–Teller (BET) method at 77 K (ASAP 2020, USA). The morphology of samples was observed on a field-emission scanning electron microscope (Zeiss SIGMA FESEM, German). The atomic composition of samples was elucidated by EDS microanalysis (EDAX Genesis, USA). SAXRD patterns of samples were analyzed using Cu Kα radiation (λ = 1.5406 Å) operating at 36 kV and 30 mA, respectively (XPert Pro, Netherlands). The FTIR analyzer was employed to determine the functional groups present for understanding the chemistry of the samples (Nicolet FTIR 5700, USA).

2.4. Analytical procedures

The pH value of solutions was determined by a Mettler-Toledo FE20 pH meter (Mettler-Toledo Instruments Co., Ltd. Shanghai). Chemical oxygen demand (COD) was measured using a fast digestion-spectrophotometric method based on the Standard of the People's Republic of China for Environmental Protection (HJ/T 399-2007) [41]. Hydrogen peroxide was analyzed spectrophotometrically with titanium oxalate [42]. Iron leaching after catalytic tests was evaluated by phenanthroline spectrophotometry [43].

2.5. Adsorption and heterogeneous photo-Fenton degradation of RhB

The experimental set-up was illustrated in Fig. S1. The adsorption experiments were carried out by immersing various weight of Fe-B in 200 mL of RhB solution at room temperature in dark. The suspension was magnetically stirred at a constant rate overnight to achieve the adsorption/desorption equilibrium between the solution and catalyst. After reaching the adsorption equilibrium, samples were withdrawn and filtrated with 0.45 μm filter membranes to determine the RhB concentration (C_e) on a UV–vis spectrophotometer (Rayleigh UV-9100) at the maximum absorption wavelength of 554 nm. The visible light photo-Fenton degradation experiments were conducted with the LED lamps as light source after overnight adsorption. The spectrum of LED lamps was shown in Fig. S2. The central wavelength and the average light intensity of LED lamps were 455 nm and 0.47 mW cm^{-2}, respectively. The reaction was initiated by adding H_2O_2 and switching on the LED lamps under magnetic stirring conditions. At given time intervals, samples were withdrawn and filtered with 0.45 μm filter membranes for the determination of RhB concentration.

The amount of dye adsorbed on a certain amount of catalyst q (mg g^{-1}) was determined according to the following equation:

$$q = (C_0 - C_e) \times \frac{V}{m} \quad (1)$$

where C_0 and C_e were the initial and adsorption equilibrium concentrations of RhB, respectively (mg L^{-1}). V was the volume of the dye solution (L) and m was the mass of catalyst (g).

The removal efficiency of RhB by adsorption (η_A) can be calculated as follows,

$$\eta_A\,(\%) = \frac{C_0 - C_e}{C_0} \times 100 \quad (2)$$

The total removal efficiency of RhB by adsorption and visible light photo-Fenton degradation (η_T) was obtained by the following equation:

$$\eta_T\,(\%) = \frac{C_0 - C}{C_0} \times 100 \quad (3)$$

where C (mg L^{-1}) was RhB concentration after visible light photo-Fenton degradation.

The removal efficiency of RhB by visible light photo-Fenton degradation (η_D) was the difference between η_T and η_A.

3. Results and discussion

3.1. Characterization of Fe-B

The nitrogen adsorption/desorption isotherms of bentonite and Fe-B shown in Fig. 1 illustrated a typical type IV pattern with a bend of volume adsorption of nitrogen at P/P_0 about 0.45 with a H-type

hysteresis loop, indicating the presence of mesoporous structure. The BET specific surface area and pore volume were 15.1 $m^2\ g^{-1}$ and 0.045 $cm^2\ g^{-1}$ for bentonite, 63.2 $m^2\ g^{-1}$ and 0.067 $cm^2\ g^{-1}$ for Fe-B, respectively. The average pore size of bentonite and Fe-B was, respectively measured as 11.9 nm and 4.2 nm. This might be attributed to the intercalation of iron into Fe-B, increasing the specific surface area of Fe-B [44].

Fig. 2(A) illustrated the SEM images of bentonite and Fe-B. It can be seen from Fig. 2 that bentonite had a layer structure; however, the support of iron led to relatively small particles and some coarse pores on the surface of Fe-B, inducing partial exfoliation of bentonite (Fig. 2(B)). The SAXRD patterns of bentonite and Fe-B were shown in Fig. 3. As can be seen from the figure, the interlayer spacing of bentonite, namely d_{001}, was 1.50 nm, indicating the bentonite was a typical kind of calcium bentonite [45,46]. With support of iron, the value of d_{001} was 1.57 nm. This change of d_{001}-value might be indicative to the intercalation of iron compounds to the interlayer region of bentonite, opening the layered structure [47,48].

The soluble ferric ion was fixed to the clay support by a process involving intercalation reaction, where the chemical bonds on the surface of solid played a significant role. Thus the FTIR spectroscopy was employed to investigate the change of functional groups on the solid surface by intercalation process. Fig. 4 showed the FTIR spectra obtained for bentonite, Fe-B and Fe_2O_3, where Fe_2O_3 was synthesized by the report of literature [49]. The peak at 3643 cm^{-1} in the two samples of bentonite and Fe-B was due to the stretching vibration of clay lattice —OH. The absorption bands at 3416 and 1614 cm^{-1} in all the three samples were assigned to the stretching vibration of H_2O molecules and the bending vibration of —OH groups attached to the adsorbed water interlayer, respectively. It can be seen that the peaks on Fe-B were analogical to those of bentonite except for the peak at 1380 cm^{-1}. The small absorption band at 1380 cm^{-1} in Fe-B catalyst spectrum referred to the bending vibration of O—H bound with ferric ion present on the surface of Fe-B [50,51]. This band existed in Fe-B was also noticeable in the spectrum of Fe_2O_3. The observation suggested that the iron was successfully embedded into the layer structure of Fe-B by the process involving reaction. Similar results were also reported by Zhang et al. [37] and Soon and Hameed [51]. For bentonite and Fe-B, the highest bands observed at approximately 1017 cm^{-1} were corresponding to asymmetric stretching vibrations of Si—O—Si bonds. Meanwhile the peak at 810 cm^{-1} existed in the above two samples belonged to symmetric stretching vibration of Si—O—Si [52].

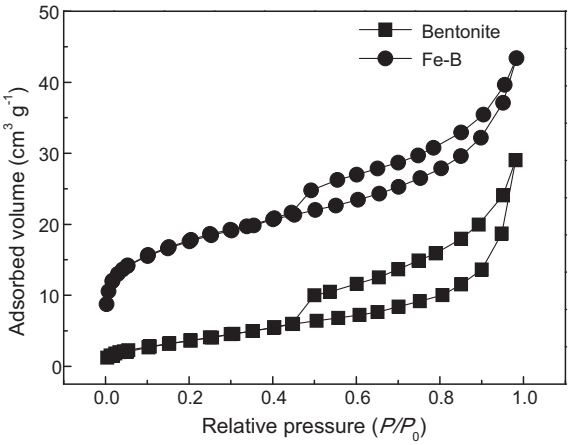

Fig. 1. Nitrogen adsorption/desorption isotherms of bentonite and Fe-B at 77 K.

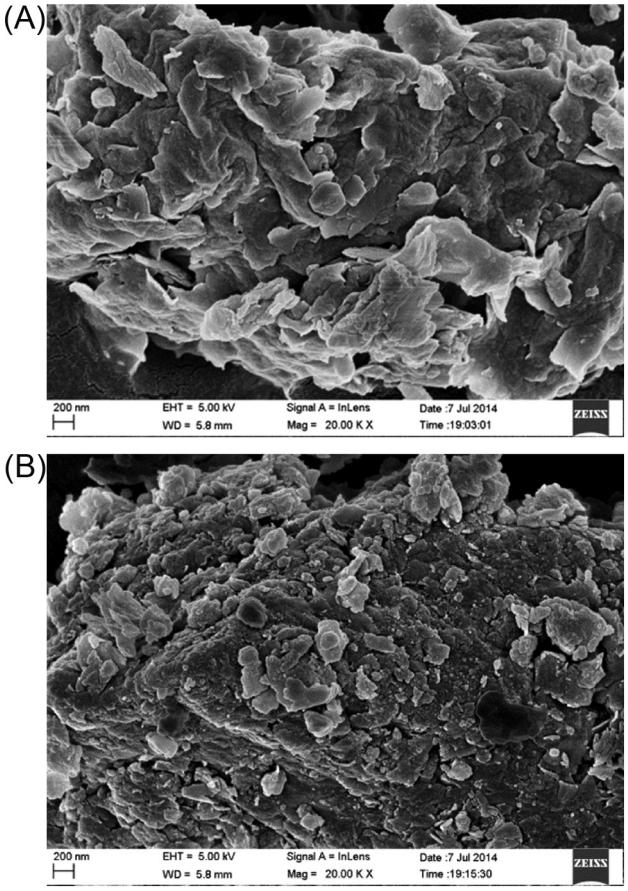

Fig. 2. SEM images of (A) bentonite and (B) Fe-B.

3.2. Adsorption characteristics of Fe-B

The adsorption was firstly conducted at various initial concentration of RhB (20 to 160 mg L^{-1}) with a Fe-B dosage of 0.25 g L^{-1} and a natural pH of 4.2. As can be seen in Fig. S3, the amount of adsorbed RhB on Fe-B (q) increased sharply from 77.06 to 197.71 mg g^{-1} when initial dye concentration increased from 20 to 80 mg L^{-1}. Further increase in the initial dye concentration did not show significant improvement in the adsorption of RhB, owing to the saturation of sorption sites on the surface of Fe-B [53]. As illustrated in Fig S3, the amount of adsorbed dye increased to only 210.27 mg g^{-1} when initial dye concentration rose to 160 mg L^{-1}.

The effect of Fe-B dosage on the adsorption of RhB was investigated by varying the amount of Fe-B in the range of 0.125–1.0 g L^{-1}

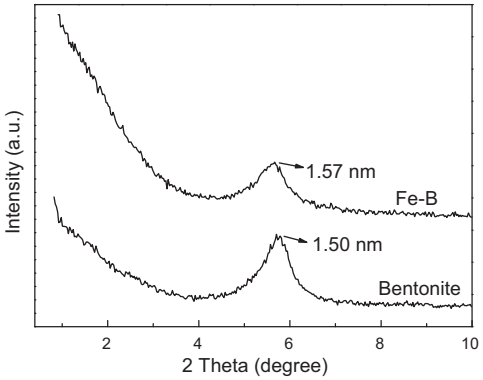

Fig. 3. Small angle XRD patterns of bentonite and Fe-B.

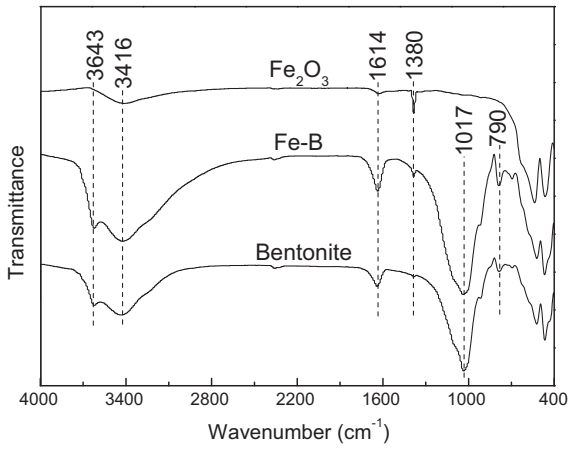

Fig. 4. FTIR spectra of bentonite, Fe-B and Fe_2O_3.

and the results were shown in Fig. 5(A). It can be seen that the removal efficiency of RhB was improved from 32% to 89% by increasing the dosage of Fe-B from 0.15 to 1.0 g L^{-1}. This could be attributed to an increase of the catalyst surface area and to the availability of more sorption sites on account of the increase of the catalyst dosage [54–56]. However, the adsorption capacity of Fe-B for RhB increased firstly and then decreased with the increase of Fe-B dosage. The maximum adsorption capacity of Fe-B was achieved with the Fe-B dosage of 0.25 g L^{-1}. Further increase in the catalyst dosage did not distinctly increase the RhB removal efficiency but decrease the adsorption capacity remarkably, on account of the split in the flux or the concentration gradient between RhB concentrations in the solution and on the Fe-B surface [55,56]. The pH parameter is an important factor significantly affecting the adsorption process. Fig. 5(B) demonstrated the amount of RhB adsorbed on Fe-B at different initial pHs ranging from 3.0 to 9.0. As depicted, the removal efficiency of RhB was decreased from 66% to 35% by increasing the initial solution pH from 3.0 to 9.0. The change of pH would affect not only the molecular speciation of RhB in aqueous solution, but also the surface charge state of Fe-B. The surface charge of Fe-B was determined by the potentiometric method [57,58]. As can be observed in Fig. 5(C), the point of zero charge (pH_{PZC}) of Fe-B was found to be 2.9 given by the intersection of titration curve with *x*-axis. Therefore, the surface of Fe-B was negatively charged at all the investigated pH (3.0–9.0). With the value of dissociation constant *p*Ka = 3.7 [59], the speciation of RhB in solution at different pH values was shown in Fig. S4. The RhB molecule existed predominantly in its cationic form (RhB^+) at pH 3.0. Electrostatic attraction between positive charge of RhB and negative charge of Fe-B surfaces would facilitate the adsorption of RhB on Fe-B. At pH 4.2 and 5.0, the fraction of RhB in positive form (RhB^+) decreased, while that in zwitterion form ($RhB^{\pm}$) increased, which resulted in the decrease in RhB removal. Furthermore, RhB removal decreased continuously at pH ≥ 7.0, as the dominant speciation of RhB changed from being cationic to zwitterionic. This was mainly due to the ionization of the carboxyl groups of RhB molecule, which was detrimental for RhB adsorption [60,61].

Adsorption behavior of RhB onto Fe-B can be elucidated by adsorption isotherms. The Freundlich and Langmuir isotherm models were used to fit the data and the results were shown in Table 1. The linear forms of Freundlich and Langmuir equation can be expressed as follows [62,63]:

$$\ln q_e = \ln K_F + \left(\frac{1}{n}\right) \times \ln C_e \quad (4)$$

$$\frac{1}{q_e} = \left(\frac{1}{q_m K_L}\right) \times \frac{1}{C_e} + \frac{1}{q_m} \quad (5)$$

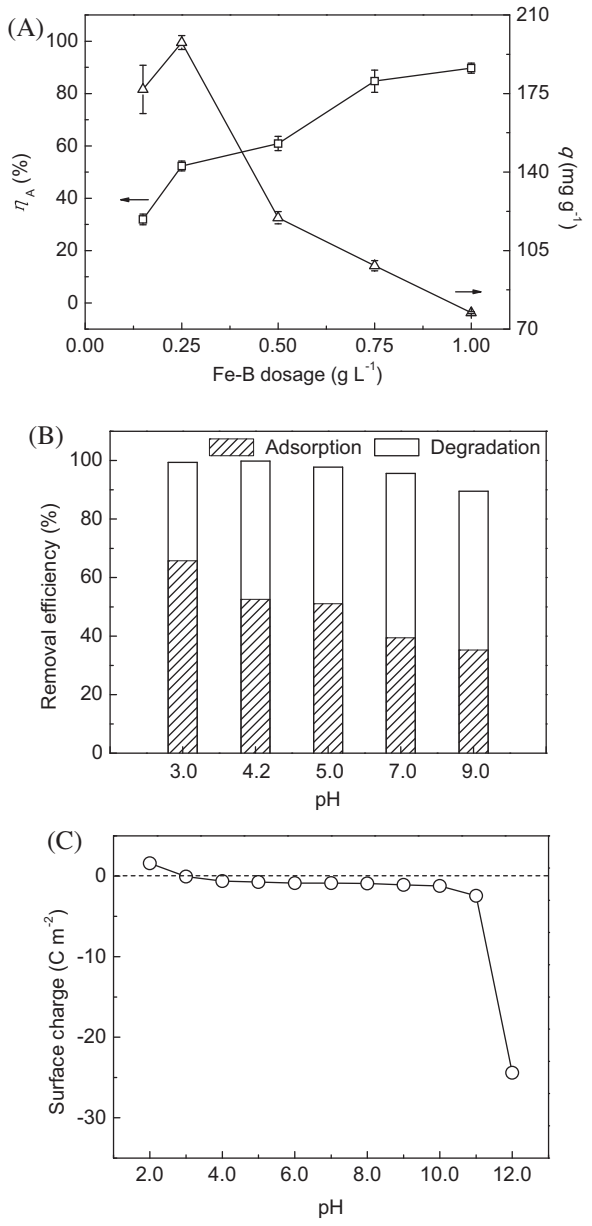

Fig. 5. (A) Effect of Fe-B dosage on the adsorption of RhB (RhB concentration: 80 mg L^{-1}; initial pH: 4.2); (B) Effect of pH on the adsorption and degradation of RhB (RhB concentration: 80 mg L^{-1}; Fe-B dosage: 0.25 g L^{-1}; H_2O_2 concentration: 12 mM); (C) Surface charge density curve of Fe-B.

where q_e is the equilibrium dye concentration on catalyst (mg g^{-1}), C_e is equilibrium concentration of dye in aqueous phase (mg L^{-1}), K_F is the Freundlich adsorption constant related to adsorption ability ($mg^{1-1/n}\ L^{1/n}\ g^{-1}$), $1/n$ is an empirical parameter relating adsorption intensity, K_L is the Langmuir adsorption constant related with the affinity of binding sites (L mg^{-1}), and q_m is the maximum adsorption capacity of catalyst (mg g^{-1}).

As can be seen from Table 1, the adsorption of RhB onto Fe-B is fitted better by the Langmuir model with the correlation

Table 1
Freundlich and Langmuir isotherm constants for RhB adsorption onto Fe-B.

isotherm model	K_F ($mg^{1-1/n}\ L^{1/n}\ g^{-1}$)	$1/n$	q_m (mg g^{-1})	K_L (L mg^{-1})	R^2
Freundlich	101.89	0.23	–	–	0.721
Langmuir	–	–	227.27	0.68	0.994

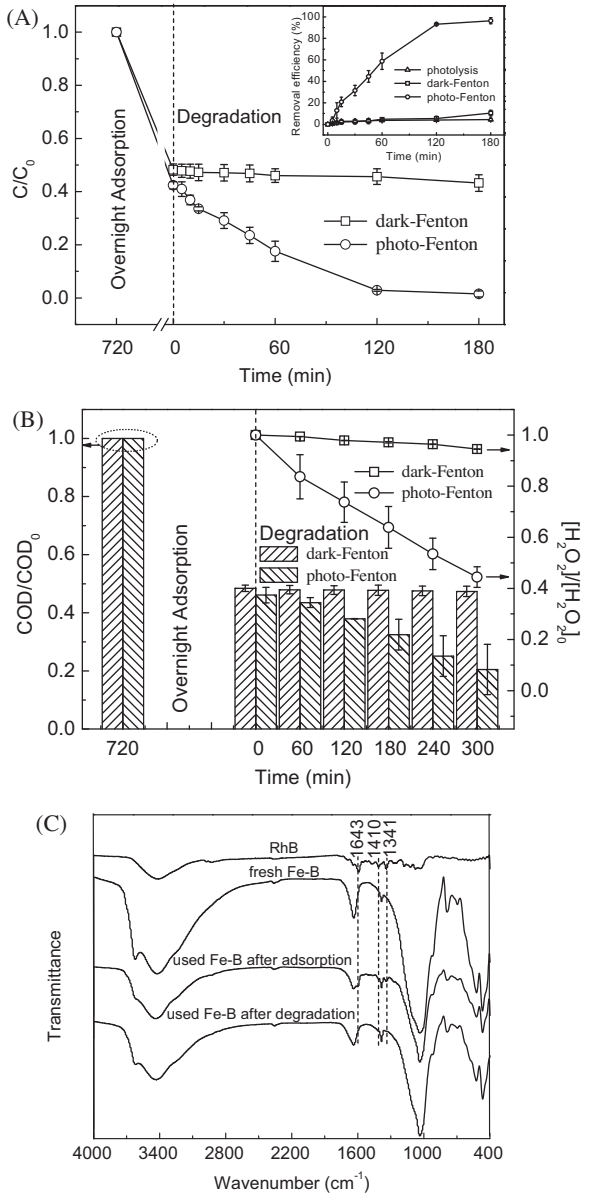

Fig. 6. (A) Removal of RhB in various processes (RhB concentration: 80 mg L^{-1}; Fe-B dosage: 0.25 g L^{-1}; initial pH: 4.2; H_2O_2 concentration: 12 mM); (B) Variation of COD and H_2O_2 in various processes (RhB concentration: 80 mg L^{-1}; Fe-B dosage: 0.25 g L^{-1}; initial pH: 4.2; H_2O_2 concentration: 12 mM); (C) FTIR spectra of samples.

coefficient of $R^2 = 0.994$, indicating that the adsorption of RhB using Fe-B occurred at the binding sites on the surface of catalyst, which is perceived as monolayer adsorption. The maximum adsorption capacity and Langmuir adsorption constant were found to be 227.27 mg g^{-1} and 0.68 L mg^{-1}, respectively.

3.3. Visible light photo-Fenton catalytic activity of Fe-B

To investigate the role of visible light in the heterogeneous photo-Fenton process, the removal of RhB in dark Fenton and visible light photo-Fenton systems was performed firstly. As can be seen in Fig. 6(A), after overnight adsorption, the addition of H_2O_2 in the dark condition resulted in little removal of RhB (5%), but under visible light irradiation, the removal efficiency of RhB increased to 41%. It indicated the important role of visible light in the heterogeneous Fenton process for the degradation of RhB. The quantum yield (Φ) was estimated to examine the photodegradation efficiency [39,64], which was found to be $(1.66 \pm 0.21) \times 10^{-2}$ (see Supplementary Material for detail). In order to explore the contribution of photolysis to the removal of RhB, the dye was irradiated by visible light alone, with the adsorption equilibrium concentration of RhB being selected as the initial dye concentration. The inset of Fig. 6(A) showed that less than 5% color removal was achieved, indicating RhB was resistant to photolysis under visible irradiation alone.

To investigate the degradation of RhB during heterogeneous photo-Fenton process, the removal of COD was also monitored and illustrated in Fig. 6(B). As can be expected, dark-Fenton process led to little COD removal (1%). This can be indirectly verified by the fact that less than 6% H_2O_2 was decomposed in this case. Under the irradiation of visible light, the COD removal efficiency was observed to increase to 80% after 300 min reaction. This could be explained by the fact that the dye molecule of RhB can absorb visible light energy and be activated to the excited state via Eq. (6). Then the excited dye molecule can transfer an electron to Fe(III) to generate Fe(II), which can promote Fe(III)/Fe(II) cycle, as given in Eq. (7) [35,36]. The generated Fe(II) could activate H_2O_2 to form $^{\bullet}OH$ radical, a strong oxidizing species with oxidation potential of 2.8 V vs. NHE, leading to the degradation of RhB as given by Eqs. (8) and (9) [35].

$$\text{Dye} + \text{visible light} \rightarrow \text{Dye}^{*} \quad (6)$$

$$\text{Dye}^{*} + \text{Fe(III)} \rightarrow \text{Fe(II)} + \text{Dye}^{+\bullet} \quad (7)$$

$$\text{Fe(II)} + H_2O_2 \rightarrow \text{Fe(III)} + {}^{\bullet}OH + OH^{-} \quad (8)$$

$$^{\bullet}OH + \text{Dye}/\text{Dye}^{+\bullet} \rightarrow \text{degradation products} \quad (9)$$

After 300 min reaction, only 44% of H_2O_2 was remained in the system. Defining the efficiency of hydrogen peroxide as the amount COD converted per unit mass of H_2O_2 decomposed:

$$E(\%) = \frac{\Delta \text{COD}}{0.47 \times \Delta[H_2O_2]} \times 100 \quad (10)$$

where ΔCOD was the removable COD value (mg L^{-1}), $\Delta[H_2O_2]$ was the decomposed H_2O_2 value (mg L^{-1}), and 0.47 is the conversion factor [65].

The E values of visible light photo-Fenton and dark-Fenton process were calculated to be 48% and 18%, respectively. As anticipated, the efficiency of hydrogen peroxide in visible light photo-Fenton process was much higher than that of dark-Fenton process.

To verify whether or not the adsorbed RhB was degraded, samples of RhB, fresh Fe-B, used Fe-B after adsorption, and used Fe-B after degradation were investigated by means of FTIR spectrometry. The FTIR spectra of the samples were shown in Fig. 6(C). As compared with the FTIR spectrum of fresh Fe-B, the new absorption peaks at 1643, 1410 and 1341 cm^{-1} and the new absorption region from 1420 to 1600 cm^{-1} appeared in the spectrum of used Fe-B after adsorption. The peaks at 1643, 1410 and 1341 cm^{-1} were, respectively attributed to the bending vibration of C=N^{+} and CH_2 in —$N^{+}(C_2H_5)_2$ and stretching vibration of C—N linked by benzene ring [37]. The new peaks and the new absorption region were consistent with the characteristic absorption peaks and region of chemical bonds or functional groups of RhB, suggesting the adsorption of RhB on the surface of Fe-B. The disappearance of the resulting peaks and region in the spectrum of used Fe-B after visible light photo-Fenton process indicated that the degradation of adsorbed RhB indeed occurred under the irradiation of visible light.

The samples of fresh Fe-B, used Fe-B after adsorption, and used Fe-B after degradation were further characterized by EDS microanalysis. As can be seen in Fig. S5, neither element N nor Cl was detected in fresh Fe-B. After overnight adsorption, the contents of N and Cl in used Fe-B increased to 3.04 wt% and 1.00 wt%, respectively. This showed that RhB was adsorbed on the surface of Fe-B, considering RhB molecule contains two nitrogen atoms and one

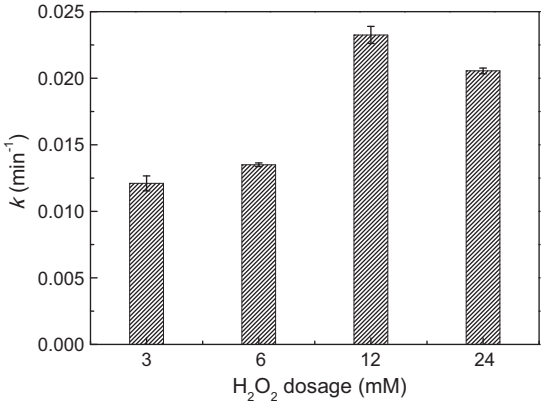

Fig. 7. Effect of H_2O_2 dosage on the degradation of RhB (RhB concentration: 80 mg L^{-1}; Fe-B dosage: 0.25 g L^{-1}; initial pH: 4.2).

chlorine atom. The N and Cl contents in used Fe-B after degradation decreased to 0.99 wt% and 0.50 wt%, respectively. It indicated that the adsorbed RhB was degraded in the presence of visible light radiation and H_2O_2, and the undesirable existence of the two elements in used Fe-B after degradation was probably attributed to the adsorption of the degradation intermediates containing N or Cl.

As discussed previously, although the adsorption of RhB on Fe-B was significantly affected by the initial pH, the degradation of RhB in visible light photo-Fenton process remained efficient at all the investigated pH values (3.0–9.0). This suggested that the application of Fe-B in visible light photo-Fenton process can overcome the drawback of a narrow pH range of conventional Fenton reaction and extend the pH range to the alkaline region. The result is consistent with the work by Catrinescu et al. [66] who reported that the clay-based catalyst could extend the range of pH values for Fenton-type oxidation. It could be attributed to the electronegativity and surface acidity of the clay-based catalysts [66,67]. It is worth noting that the solution pH changed during the degradation process. Table S1 indicated that the pH value dropped from the initial pH of 4.2 to approximate 3.6 after 300 min photodegradation. The same change trend in pH was observed at initial pH > 4.2, in which, the pH decreased to 3.8, 4.2 and 4.8 at the end of the reaction when the initial pH values were 5.0, 7.0 and 9.0, respectively. The formation of intermediates such as carboxyl acids accounted for the decrease of pH, which was favorable for the Fenton reaction [68,69]. Since Fe-B displayed a reasonable good photocatalytic activity at natural pH 4.2, the photo-Fenton experiments could be performed without pre-adjusting their pH values. In addition, the good photocatalytic activity of Fe-B was also maintained when the initial pH of the solution was 5.0–9.0. It indicated that the photo-Fenton process could be efficient at circumneutral pH or even basic conditions.

The effect of H_2O_2 dosage was examined on the visible light photocatalytic activity of Fe-B by varying initial H_2O_2 concentration from 3 to 24 mM. The removal of RhB followed pseudo-first-order kinetics with correlation coefficients ranging from 0.974 to 0.993. As shown in Fig. 7, the apparent rate constant (k) increased from 0.012 to 0.023 min^{-1} when H_2O_2 concentration increased from 3 to 12 mM. This demonstrated that more hydroxyl radicals were generated with the increase of concentration of H_2O_2. However, further increase of H_2O_2 to 24 mM led to a slight decrease of the k value. This might be due to the fact that excessive H_2O_2 behaving as a scavenger of hydroxyl radical would suppress the degradation rate [30]. The similar observations have been reported by other researchers [44,70,71].

In order to verify the role of hydroxyl radical playing in the degradation of RhB in the photo-Fenton process under visible light

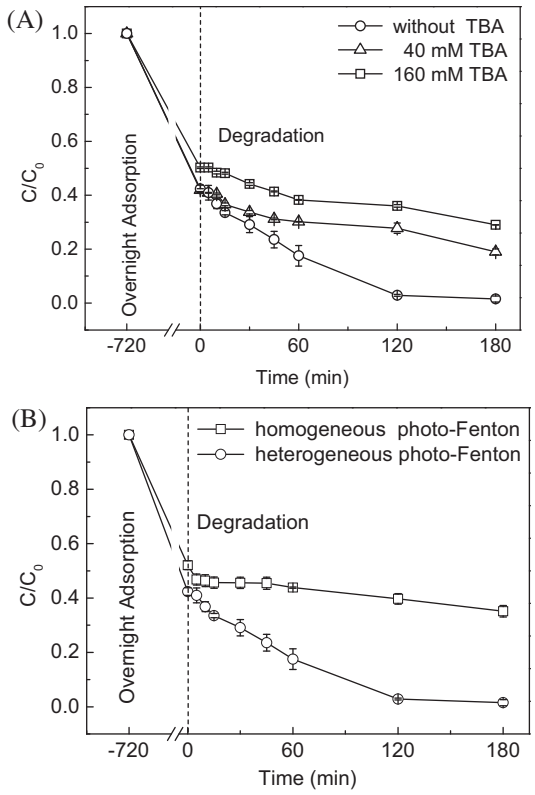

Fig. 8. (A) Effect of scavenger on the degradation of RhB (RhB concentration: 80 mg L^{-1}; Fe-B dosage: 0.25 g L^{-1}; initial pH: 4.2; H_2O_2 concentration: 12 mM); (B) Effect of leaching iron on the degradation of RhB (RhB concentration: 80 mg L^{-1}; Fe-B dosage: 0.25 g L^{-1}; initial pH: 4.2; H_2O_2 concentration: 12 mM).

irradiation, *tert*-butyl alcohol (TBA), known as a typical scavenger for hydroxyl radical, was employed in the experiments. As can be seen in Fig. 8(A), the removal efficiency of RhB by visible light photo-Fenton process decreased by 18% after adding 40 mM TBA. Further increasing TBA concentration to 160 mM reduced the removal efficiency of RhB by 28%. It elucidated that the presence of excessive TBA decreased the degradation rate of RhB, revealing that hydroxyl radical played an important role in the degradation of RhB in the visible light photo-Fenton process.

To evaluate the contribution of the homogeneous Fenton reaction catalyzed by leached iron from the solid to aqueous media, the solid catalyst was removed after the adsorption stage by means of centrifugation. And then, the equal amount of H_2O_2 was added into the supernatant to start the reaction under the irradiation of visible light. It can be clearly observed from Fig. 8(B) that the homogeneous photo-Fenton process resulted in a very limited removal of RhB. It indicated that the RhB degradation was mainly attributed to the heterogeneous photo-Fenton reaction. Moreover, the relatively low leaching percentage of iron (7%) at pH 3.0 confirmed the good chemical stability of Fe-B and consequently the contribution of this leached iron to overall catalytic activity was considered negligible.

3.4. Stability of Fe-B in visible light photo-Fenton process

The stability of Fe-B was investigated by means of recycling experiments. The Fe-B catalyst was repeatedly applied to remove RhB by successive batch experiments. After each run, Fe-B remained in the reaction solution was centrifugally separated and then oven dried at 100 °C overnight. The same amount of dried powder was used as a catalyst for the next batch experiment. As can be observed in Fig. 9, Fe-B was capable of being reutilized for at least five cycles, and the reused catalyst almost retained efficient photocatalytic activity. After the fifth cycle, the total removal

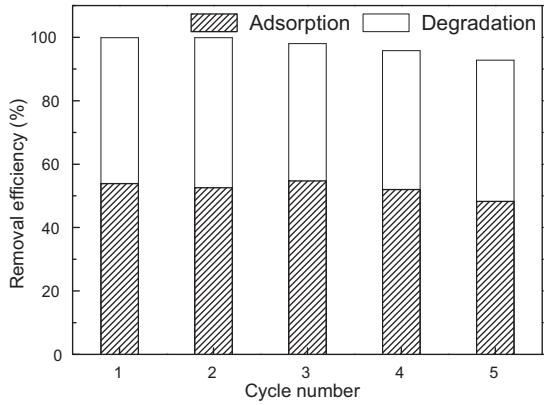

Fig. 9. Catalyst recycling in the removal of RhB (RhB concentration: 80 mg L^{-1}; Fe-B dosage: 0.25 g L^{-1}; initial pH: 4.2; H_2O_2 concentration: 12 mM).

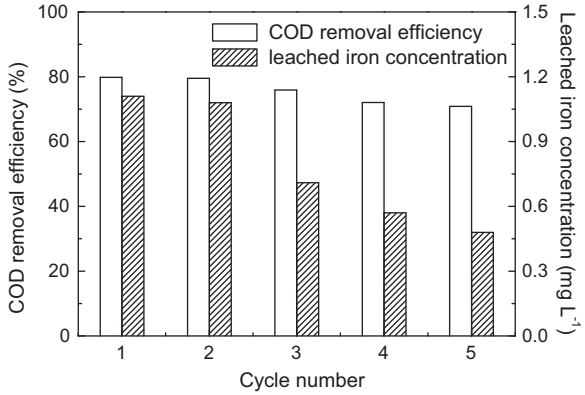

Fig. 10. Variation of COD removal efficiency and leached iron concentration as a function of cycle number.

efficiency of RhB could achieve as high as 93%. In addition to RhB removal efficiency, the COD removal efficiency and the leached iron concentration at the end of each cycle were also monitored and the results were shown in Fig. 10. It demonstrated that Fe-B remained high photocatalytic activity and stability, with 71% of the COD removal efficiency being achieved and 0.48 mg L^{-1} of iron being leached after the fifth cycle. The results above indicated that Fe-B could behave as a stable and efficient heterogeneous photo-Fenton catalyst for removal of RhB by combination of adsorption and degradation in the presence of visible light irradiation and H_2O_2.

4. Conclusions

Fe-B catalyst was successfully prepared by a facile method. The support of iron obviously increased the specific surface area of Fe-B and consequently enhanced the adsorption affinity of Fe-B toward RhB from aqueous phase. Accompanying the good adsorption ability, the prepared Fe-B exhibited excellent photocatalytic activity and high chemical stability with wide operating range of pH in the visible light photo-Fenton process. The use of the inexpensive Fe-B and visible LED lamps reduced the cost of starting materials and experimental setup in addition to convenient operation and lower power consumption. We believe that Fe-B could be used as an efficient heterogeneous photo-Fenton catalyst for the treatment of dye-containing wastewater by means of adsorption and degradation with the simultaneous use of visible LED lamps and H_2O_2. Future work will focus on toxicity issues so that the effluent could be safely discharged into receiving water bodies.

Acknowledgment

This work was supported by Natural Science Foundation of Hubei Province, China (Grant 2012FFA089).

Appendix A. Supplementary data

Supplementary material related to this article can be found, in the online version, at http://dx.doi.org/10.1016/j.apcatb.2014.11.005.

References

[1] R. Salazar, E. Brillas, I. Sirés, Appl. Catal., B: Environ. 115 (2012) 107–116.
[2] S. Tian, J. Zhang, J. Chen, L. Kong, J. Lu, F. Ding, Y. Xiong, Ind. Eng. Chem. Res. 52 (2013) 13333–13341.
[3] C. Cai, H. Zhang, X. Zhong, L. Hou, Water Res. 66 (2014) 473–485.
[4] S. Horikoshi, F. Hojo, H. Hikaka, N. Serpone, Environ. Sci. Technol. 38 (2004) 2198–2208.
[5] S. Guo, G. Zhang, J. Wang, J. Colloid Interface Sci. 433 (2014) 1–8.
[6] I. Konstantinou, T. Albanis, Appl. Catal., B: Environ. 49 (2004) 1–14.
[7] M. Asiltürk, F. Sayilkan, S. Erdemoğlu, M. Akarsu, H. Sayılkan, M. Erdemoğlu, E. Arpac, J. Hazard. Mater. 129 (2006) 164–170.
[8] H. Zabova, V. Cirkva, J. Chem. Technol. Biotechnol. 84 (2009) 1624–1630.
[9] J. Clark, M. Dyer, R. Palgrave, C. Ireland, J. Darwent, J. Claridge, M. Rosseinsky, J. Am. Chem. Soc. 133 (2011) 1016–1032.
[10] H. Fu, C. Pan, W. Yao, Y. Zhu, J. Phys. Chem. B 109 (2005) 22432–22439.
[11] S. Yan, Z. Li, Z. Zou, Langmuir 26 (2010) 3894–3901.
[12] Y. Wang, S. Li, X. Xing, F. Huang, Y. Shen, A. Xie, X. Wang, J. Zhang, Chem. Eur. J. 17 (2011) 4802–4808.
[13] X. Yang, C. Cao, L. Erickson, Appl. Catal., B: Environ. 91 (2009) 657–662.
[14] Y. Wang, Y. Su, L. Qiao, L. Liu, Q. Su, C. Zhu, X. Liu, Nanotechnology 22 (2011) 225702–225709.
[15] F. Wang, K. Zhang, J. Mol. Catal. A: Chem. 345 (2011) 101–107.
[16] M. Perez, F. Torradesa, X. Domenechb, J. Peral, Water Res. 36 (2002) 2703–2710.
[17] E. Garrido-Ramírez, B. Theng, M. Mora, Appl. Clay Sci. 47 (2010) 182–192.
[18] H. Zhang, H. Choi, C. Huang, J. Hazard. Mater. 136 (2006) 618–623.
[19] Y. Huang, Y. Huang, P. Chang, C. Chen, J. Hazard. Mater. 154 (2008) 655–662.
[20] J. Herney-Ramirez, M. Vicente, L. Madeira, Appl. Catal., B: Environ. 98 (2010) 10–26.
[21] Y. Gong, H. Zhang, Y. Li, L. Xiang, S. Royer, S. Valange, J. Barrault, Water Sci. Technol. 62 (2010) 1320–1326.
[22] H. Zhang, X. Wu, X. Li, Chem. Eng. J. 210 (2012) 188–194.
[23] H. Zhang, H. Gao, C. Cai, C. Zhang, L. Chen, Water Sci. Technol. 68 (2013) 2515–2520.
[24] S. Chou, C. Huang, Chemosphere 38 (1999) 2719–2731.
[25] C. Hsueh, Y. Huang, C. Chen, J. Hazard. Mater. 129 (2006) 228–233.
[26] M. Kasiri, H. Aleboyeh, A. Aleboyeh, Appl. Catal., B: Environ. 84 (2008) 9–15.
[27] R. Gonzalez-Olmos, U. Roland, H. Toufar, F. Kopinke, A. Georgi, Appl. Catal., B: Environ. 89 (2009) 356–364.
[28] A. Pham, C. Lee, F. Doyle, D. Sedlak, Environ. Sci. Technol. 43 (2009) 8930–8935.
[29] R. Gonzalez-Olmos, M. Martin, A. Georgi, F. Kopinke, I. Oller, S. Malato, Appl. Catal., B: Environ. 125 (2012) 51–58.
[30] S. Guo, G. Zhang, Y. Guo, J. Yu, Carbon 60 (2013) 437–444.
[31] T. Manjot, J. Bo, Chem. Eng. J. 187 (2008) 79–88.
[32] A. Gil, F. Assis, S. Albeniz, S. Korili, Chem. Eng. J. 168 (2011) 1032–1040.
[33] J. Herney-Ramirez, M. Lampinen, M. Vicente, C. Costa, L. Madeira, Ind. Eng. Chem. Res. 47 (2008) 284–294.
[34] N. Daud, M. Ahmad, B. Hameed, Chem. Eng. J. 165 (2010) 111–116.
[35] M. Cheng, W. Song, W. Ma, C. Chen, J. Zhao, J. Lin, H. Zhu, Appl. Catal., B: Environ. 77 (2008) 355–363.
[36] Q. Chen, P. Wu, Y. Li, N. Zhu, Z. Dang, J. Hazard. Mater. 168 (2009) 901–908.
[37] G. Zhang, Y. Gao, Y. Zhang, Y. Guo, Environ. Sci. Technol. 44 (2010) 6384–6389.
[38] W. Jo, R. Tayade, Ind. Eng. Chem. Res. 53 (2014) 2073–2084.
[39] J. Xu, J. Li, F. Wu, Y. Zhang, Environ. Sci. Technol. 48 (2014) 272–278.
[40] J. Feng, X. Hu, P. Yue, Environ. Sci. Technol. 38 (2004) 269–275.
[41] National General Administration of Environmental Protection, Water Quality–Determination of the Chemical Oxygen Demand–Fast Digestion–Spectrophotometric Method (HJ/T 399–2007), Environmental Science Press of China, Beijing, 2007 (in Chinese).
[42] R. Sellers, Analyst 105 (1980) 950–954.
[43] National General Administration of Environmental Protection, Water Quality–Determination of Iron–Phenanthroline Spectrophotometry (HJ/T 345–2007), Environmental Science Press of China, Beijing, 2007 (in Chinese).
[44] O. Ayodele, B. Hameed, J. Ind. Eng. Chem. 19 (2013) 966–974.
[45] H. Zhang, Z. Tong, T. Wei, Y. Tang, Appl. Clay Sci. 65 (2012) 21–23.
[46] N. Sanabria, R. Molina, S. Moreno, J. Adv. Oxid. Technol. 15 (2012) 117–124.
[47] M. Luo, D. Bowden, P. Brimblecombe, Appl. Catal., B: Environ. 85 (2009) 201–206.
[48] X. Zhao, L. Zhu, Y. Zhang, J. Yan, X. Lu, Y. Huang, H. Tang, J. Hazard. Mater. 215–216 (2012) 57–64.

[49] Y. Wang, J. Xu, H. Wu, M. Xu, Z. Peng, G. Zheng, J. Mater. Chem. 22 (2012) 21923–21927.
[50] Q. Zhang, W. Jiang, H. Wang, M. Chen, J. Hazard. Mater. 176 (2010) 1058–1064.
[51] A. Soon, B. Hameed, Appl. Catal., A: Gen. 450 (2013) 96–105.
[52] M. Timofeeva, S. Khankhasaeva, Y. Chesalov, S. Tsybulya, V. Panchenko, E. Dashinamzhilova, Appl. Catal., B: Environ. 88 (2009) 127–134.
[53] Y. Bulut, H. Aydin, Desalination 194 (2006) 259–267.
[54] M. Entezari, Z. Al-Hoseini, Ultrason. Sonochem. 14 (2007) 599–604.
[55] O. Hamdaoui, M. Chiha, E. Naffrechoux, Ultrason. Sonochem. 15 (2008) 799–807.
[56] H. Li, X. Zhong, H. Zhang, L. Xiang, S. Royer, S. Valange, J. Barrault, Water Sci. Technol. 69 (2014) 819–824.
[57] J. Chen, M. Lin, Water Res. 35 (2001) 2385–2394.
[58] W. Xiong, J. Peng, Water Res. 42 (2008) 4869–4877.
[59] T. Saleh, V. Gupta, J. Colloid Interface Sci. 362 (2011) 337–344.
[60] M. Cheng, W. Ma, C. Chen, J. Yao, J. Zhao, Appl. Catal., B: Environ. 65 (2006) 217–226.
[61] S. Su, W. Guo, Y. Leng, C. Yi, Z. Ma, J. Hazard. Mater. 244–245 (2013) 736–742.
[62] H. Freundlich, Z. Phys. 57 (1906) 385–470.
[63] I. Langmuir, J. Am. Chem. Soc. 40 (1918) 1361–1403.
[64] D. Zhou, L. Chen, C. Zhang, Y. Yu, L. Zhang, F. Wu, Water Res. 57 (2014) 87–95.
[65] Y. Kang, K. Hwang, Water Res. 34 (2000) 2786–2790.
[66] C. Catrinescu, C. Teodosiu, M. Macoveanu, J. Miehe-Brendlé, R. Dred, Water Res. 37 (2003) 1154–1160.
[67] J. Chen, L. Zhu, Chemosphere 65 (2006) 1249–1255.
[68] J. Feng, X. Hu, P. Yue, Water Res. 40 (2006) 641–646.
[69] W. Najjar, S. Azabou, S. Sayadi, A. Ghorbel, Appl. Catal., B: Environ. 74 (2007) 11–18.
[70] H. Zhang, H. Fu, D. Zhang, J. Hazard. Mater. 172 (2009) 654–660.
[71] X. Zhong, L. Xiang, S. Royer, S. Valange, J. Barrault, H. Zhang, J. Chem. Technol. Biotechnol. 86 (2011) 970–977.